SAGE CRISP PUBLICATIONS DIRECTORY

Authors:-

Ou, Chang-Yu and Lai, Ching-Her

FINITE ELEMENT ANALYSIS OF DEEP EXCAVATION IN LAYERED SANDY AND CLAYEY SOIL DEPOSITS

Publication:-

CANADIAN GEOTECHNICAL JOURNAL
31, pp 204-214

Year of Publication

1994

REPRODUCED WITH KIND PERMISSION FROM:-
Canadian Geotechnical Journal
National Research Council of Canada
Ottawa
ON KIA OR6
Canada OX5 1GB

Finite-element analysis of deep excavation in layered sandy and clayey soil deposits

CHANG-YU OU

Department of Construction Engineering, National Taiwan Institute of Technology, P.O. Box 90-130, Taipei, Taiwan, Republic of China

AND

CHING-HER LAI

Geotechnical and Environmental Engineering Department, Resources Engineering Services Inc. Taipei, Taiwan, Republic of China

Received April 30, 1993

Accepted December 2, 1993

This paper presents an application of finite-element analysis to deep excavation in layered sandy and clayey soil deposits using a combination of the hyperbolic and the Modified Cam-clay models. In the analysis, the drained behavior of cohesionless soil and the undrained behavior of cohesive soil were simulated using the hyperbolic and Modified Cam-clay models, respectively. A rational procedure for determining soil parameters for each of the models was established. A simulation of the dewatering process during excavation was proposed. The analytical procedure was confirmed through an analysis of three actual excavation cases. Finally, analyses considering pore-water pressure dissipation during the actual elapsed time for each construction phase were carried out. The results indicate that the calculated displacement of a retaining wall during excavation is smaller than that given by undrained analysis. It was thought that some degree of pore-water pressure dissipation actually occurs during the intermediate excavation stages. This results in a decrease in the final deformation of the wall and ground-surface settlement than would be predicted by undrained analysis.

Key words: finite-element analysis, deep excavation, hyperbolic model, Cam-clay model.

Cet article présente une application de l'analyse en éléments finis d'une excavation profonde dans des dépôts formés de couches de sols sableux et argileux en utilisant une combinaison des modèles hyperbolique et Cam-clay modifié. Dans l'analyse, le comportement drainé du sol pulvérulent et le comportement non drainé du sol cohérent sont simulés en utilisant le modèle hyperbolique et le modèle Cam-clay modifié respectivement. Une procédure rationnelle pour déterminer les paramètres de sol pour chacun des modèles a été établie. Une simulation du processus de rabattement de nappe durant l'excavation a été proposée. La procédure analytique a été confirmée au moyen d'une analyse de trois cas réels d'excavation. Finalement, des analyses prenant en compte la dissipation de la pression interstitielle durant le temps réellement écoulé pour chaque phase de construction ont été réalisées. Les résultats indiquent que le déplacement calculé d'un mur de soutènement durant l'excavation est plus petit que celui donné par l'analyse non drainée. L'on croit qu'un certain degré de dissipation des pressions interstielles se produit effectivement au cours des phases intermédiaires d'excavation. Il en résulte une déformation finale plus petite du mur et un affaissement de la surface du terrain plus faible que les aurait prédits l'analyse non drainée.

Mots clés : analyse en éléments finis, excavation profonde, modèle hyperbolique, modèle Cam-clay.

[Traduit par la rédaction]

204–214 (1994)

Introduction

Accuracy of finite-element analysis of deep excavation depends greatly on the stress–strain model used and on the finite element formulation. The linear–elastic, linear–elastic perfectly plastic, and hyperbolic models are the most common stress–strain models of soils used in the analysis of geotechnical problems. The hyperbolic model, as proposed by Duncan and Chang (1970), can take into account the nonlinear, inelastic, and pressure-dependent behavior of soils. The model parameters can be obtained directly from conventional triaxial tests. Therefore, the hyperbolic model has been applied in the analysis of geotechnical engineering problems quite extensively. However, it is not easy to perform finite-element analysis of deep excavation considering pore-water pressure dissipation using the hyperbolic model because an additional pore-water pressure generation model has to be introduced into the formulation.

The Modified Cam-clay model, as proposed by Roscoe and Burland (1968), was derived on the basis of energy dissipation during the shearing process in the soil. The number of parameters required to describe soil behavior in the Modified Cam-clay model is less than that in the hyperbolic model. All of the model parameters can be obtained from conventional laboratory tests. If the model is incorporated with the general consolidation theory in the finite-element formulation, not only can it predict the drained and undrained behavior of the soil, but it can also simulate the pore-water pressure dissipation during excavation. However, the application of the Modified Cam-clay model for sandy soils is still in the research stage. Therefore, it is reasonable to use the Modified Cam-clay model along with the hyperbolic model for excavation analysis in layered clayey and sandy soil deposits.

However, other than the selection of a constitutive model for the soil, the most difficult aspect in applying finite-element techniques to the analysis of deep excavation is the estimation of soil parameters. The widespread use of back analysis reflects the fact that some of the soil parameters

Printed in Canada / Imprimé au Canada

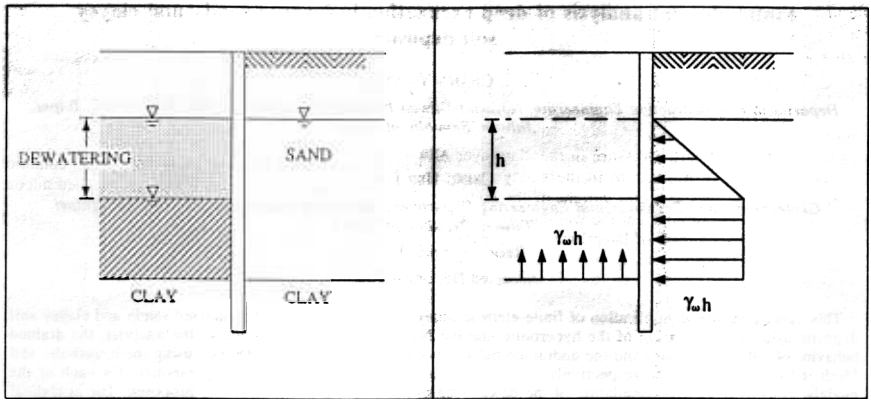

FIG. 1. Simulation of dewatering. (*a*) Dewatering in an excavation on layered sandy and clayey soils. (*b*) Model of pore-water pressure due to dewatering. *h*, dewatering depth; γ_w, unit weight of water.

are heavily affected by the effects of soil disturbance and are not suitably obtained from the laboratory test (Clough and Mana 1976). Analysis with the values from the laboratory test can lead to large differences from the observed values. For this reason, the purpose of this study is to establish a rational procedure for determining soil parameters for the finite-element analysis of deep excavations using a combination of the Modified Cam-clay and hyperbolic models instead of back analysis. Furthermore, the effects of pore-water pressure dissipation during excavation on wall deformation and ground-surface settlement are investigated.

Finite-element analysis

A modified version of the computer program JFEST, which was originally developed for simulating shield tunnelling (Finno 1983), is used as a basic research tool in this paper. The program simulates the process of digging soil during excavation using a method similar to that proposed by Ghaboussi and Pecknold (1984) and Brown and Booker (1985). The program satisfies the principle of unique solution in the elastic analysis of excavation (Ishihara 1970). To model the excavation more realistically, bar elements are included in the program to represent the lateral support such as temporary steel struts or concrete floor slabs. In addition, a simulation of the dewatering process during excavation in layered sandy and clayey soil deposits is developed in this section. The simulation of drained and undrained materials is also discussed.

Simulation of dewatering

Due to a decrease in pore-water pressure during dewatering, the retaining wall will deform toward the dewatering side. This process is simulated by applying equivalent nodal forces at the boundary between the permeable and impermeable layers and between the permeable layer and the retaining wall (see Fig. 1). The equivalent nodal forces generated by dewatering are then added to excavation terms as follows:

$$[1] \quad \{f\} = \int_V [B]^T \{U\}\, dV + \int_V [B]^T [\sigma]\, dV - \int_V [N]^T \gamma\, dV$$

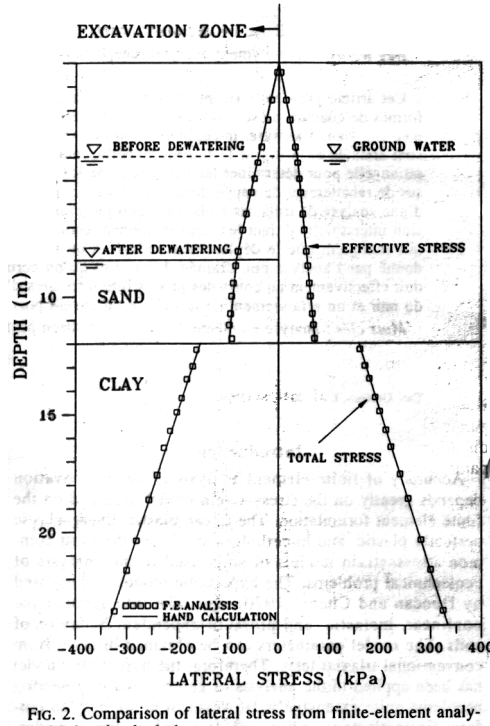

FIG. 2. Comparison of lateral stress from finite-element analysis with hand calculation.

where $\{f\}$ denotes the equivalent nodal forces; $[B]$ denotes the strain-displacement matrix; $\{U\}$ is the magnitude of decrease in pore-water pressure; $[\sigma]$ is the stress vector;

$[N]$ is the displacement shape function, $\{\gamma\}$ is body force, T is the transpose operation of a matrix; V is volume.

A building site where the groundwater level originally was 4 m below ground surface and was lowered to 8 m below ground surface was employed to verify the simulation procedure above. Since the site was not excavated, dewatering only may cause the retaining wall to deform very little. The total lateral earth pressure in the clay layer and the effective lateral earth pressure in the sandy layer can be obtained directly from the unit weight of the soils. This hand calculation does not consider the wall-deformation effect. Figure 2 shows comparison of lateral stresses against the wall from hand calculation and from finite-element analysis using the simulation procedure described above for the stratum composed of sandy and clayey soils. It is noted that the sandy and clayey soils during the analysis were simulated using the hyperbolic and Modified Cam-clay models, respectively. It can be seen from Fig. 2 that the results from both methods are in very close agreement. The simulation procedure for dewatering as proposed in the study is therefore verified.

Simulation of drained material

In this study, the behavior of cohesionless soil is modelled by the nonlinear elastic formulation as proposed by Duncan and Chang (1970). The basic idea of this model is to characterize the stress–strain response by an empirical equation, where the nonlinear stress-dependent hyperbolic curve is used for loading and a linear stress-dependent response is used for unloading and reloading. At any given stress level, a tangent modulus to the equation is used to predict the stress–strain relationship for the next loading increment. The convergence between predicted and actual responses is achieved by a number of small loading increments and special iteration techniques. There are seven parameters, such as cohesion $\bar{c}$, friction angle $\bar{\phi}$, stiffness modulus number for primary loading K, stiffness modulus exponent n, stiffness modulus number for unloading–reloading K_{ur}, failure ratio R_f, and Poisson's ratio ν_t, which are required to fully describe the stress–strain behavior of the soil in the hyperbolic model. The strength parameters $(\bar{c}, \bar{\phi})$ can be obtained directly from laboratory tests with good accuracy. However, it is not fitting to obtain the rest of the model parameters from laboratory tests due to the effect of sample disturbance. A proposed procedure for determining model parameters is described in the later sections of this paper.

Simulation of undrained material

According to the theory of plasticity, the stress increments $\{\Delta\sigma\}$ and the strain increments $\{\Delta\epsilon\}$ for an element of an elastoplastic material under plane strain conditions obey the following relationship:

$$[2] \quad \{\Delta\sigma\} = ([C^e] - [C^p])\{\Delta\epsilon\}$$

where $[C^e]$ and $[C^p]$ are elastic and plastic stress–strain matrices, respectively. The matrix $[C^p]$ is related to the yield surface of the soil. For the Modified Cam-clay model, the yield surface is a function of the slope λ of the isotropic consolidation line, the slope κ of the swelling line, and the slope M of the critical state line.

The elastic matrix $[C^e]$ can be expressed in terms of either the elastic Poisson's ratio and the elastic bulk modulus or the elastic shear modulus and the elastic bulk modulus. In this study, the elastic matrix $[C^e]$ under drained conditions is expressed as

$$[3] \quad [C^e] = \frac{1}{\Delta}\begin{bmatrix} 3\bar{B}+4G & 3\bar{B}-2G & 0 \\ 3\bar{B}-2G & 3\bar{B}+4G & 0 \\ 0 & 0 & G \end{bmatrix}$$

where $\bar{B}$ is elastic bulk modulus under drained conditions, and G is elastic shear modulus. $\bar{B}$ can be obtained according to the critical state theory:

$$[4] \quad \bar{B} = \frac{1+e}{\kappa}\bar{p}$$

where $\bar{p}$ is mean effective stress; and e is void ratio, which can be calculated from the critical void ratio e_{cs}, which is the void ratio of the one-dimensional consolidation line when $\bar{p}$ = 1.0. Therefore, there are five parameters (λ, κ, e_{cs}, M, G) required to fully describe the stress–strain behavior of the soil based on the Modified Cam-clay theory under drained conditions.

For the undrained analysis, the drained elastic bulk modulus, $\bar{B}$ in [3] must be replaced by the undrained elastic bulk modulus B. B can be obtained by summing $\bar{B}$ and the effect of water stiffness on the soil.

Britto and Gunn (1987) suggested that the undrained elastic bulk modulus B be determined as follows:

$$[5] \quad B = \bar{B} + \alpha K_w$$

where K_w is bulk modulus of water, and α is reduction factor. Finno (1983) suggested that the undrained elastic bulk modulus be estimated using the concept of equivalent porosity of soils in the following:

$$[6] \quad \frac{1}{B} = \frac{n'}{K_w} + \frac{1-n'}{\bar{B}}$$

where n' is porosity of the soil. However, it should be noted that the bulk modulus of water is very large and is difficult to estimate. Britto and Gunn (1987) suggested that the undrained analysis be performed by trying various values of the bulk modulus of water until reasonable analytical values are obtained. Inevitably, this procedure would require abundant professional experience and subjective judgement.

By replacing αK_w with B_w in [5], the equation becomes

$$[7] \quad B = \bar{B} + B_w$$

By assuming that the elastic shear modulus G is the same for both drained and undrained conditions, then

$$[8] \quad G = \frac{\bar{E}}{2(1+\bar{\nu})} = \frac{E}{2(1+\nu)}$$

$$[9] \quad \bar{B} = \frac{\bar{E}}{3(1-2\bar{\nu})}$$

$$[10] \quad B = \frac{E}{3(1-2\nu)}$$

where $\bar{E}$ and E are drained and undrained elastic Young's moduli, respectively; and $\bar{\nu}$ and ν are drained and undrained Poisson's ratios, respectively. From [7]–[10], the following relationship can be obtained:

$$[11] \quad B_w = \left[\frac{(1+\nu)(1-2\bar{\nu})}{(1+\bar{\nu})(1-2\nu)} - 1\right]\bar{B}$$

TABLE 1. Model parameters for the Chi-Ching building site

Soil parameter	Silty sand (0–12 m)	Silty clay (12–16 m)	Silty clay (16–24 m)	Silty sand or clayey silt (24–50 m)
M	—	1.11	1.11	—
λ	—	0.19	0.148	—
κ	—	0.038	0.03	—
e_{cs}	—	1.3	1.3	—
G/S_u	—	180	300	—
$\bar{\nu}$	—	0.3	0.3	—
ν	—	0.49	0.49	—
$\bar{c}$ (kPa)	0.0		—	0.0
$\bar{\phi}$ (°)	31	—		32.5
R_f	0.7	—	—	0.7
ν_i	0.3	—	—	0.3
ν_f	0.49	—	—	0.49
K	550			1200
n	0.5	—		0.5
K_{ur}	550	—		1200

NOTE: ν_f is Poisson's ratio at or near failure.

By replacing $\bar{B}$ with B in [3], the effect of water in an undrained analysis is taken into account. Therefore, there are seven parameters $\bar{\nu}$, ν, λ, κ, e_{cs}, M, and G required to fully describe the stress–strain behavior of soils for undrained analysis using the Modified Cam-clay theory.

Analysis with pore-water pressure dissipation

Small et al. (1976) derived the finite-element consolidation formula based on Biot's (Biot 1941) general consolidation theory. The finite-element formulation used in this study is based on the works of Small et al. (1976) and Johnston (1981). It will not be discussed in much detail in this paper. Required parameters for consolidation are the vertical permeability K_v, horizontal permeability K_h, and time increment Δt.

Case studies: undrained analysis

The Chi-Ching building

The Chi-Ching building is located in Taipei. The maximum excavation depth is 13.2 m below ground surface. A diaphragm wall 70 cm thick and 28 m long was used as the retaining structure. The excavation was completed using the top-down method of construction in four stages. The first three excavation stages were supported by the concrete floor slab, and the final stage was supported using temporary steel struts. The groundwater level was originally 3 m below ground surface; it was lowered to 8.4 m depth at the excavation side before the excavation was started and then lowered further to 12.0 m depth at the third excavation stage.

The building site is rectangular, but only a 32.6 m width of a section was used in this study. An inclinometer casing was placed at or near the centre of each side. Wall deformation was measured down to 26 m below the ground surface. Hydraulic earth pressure cells were installed at four different depths down the centre panel of one side. The rebar strain meters were installed in the reinforcement cages in three sections of the opposite sides to measure the deformation of reinforcement. More detailed instrumentation is given in Moh and Associates (1982).

The eight-noded quadrilateral element (Q8 element) was selected for the soil and diaphragm wall in the analysis. The diaphragm wall and lateral support are assumed to behave as a linear–elastic material. The Young's modulus of the wall used in the analysis was 1.9×10^7 kN/m^2, and the Poisson's ratio was assumed to be 0.2. The axial stiffness of the concrete slab based on the slab thickness and excavation width was 98100 kN/m. The axial stiffness of the temporary steel struts based on the strut spacing and type were and 7400 kN/m.

The ground condition at the site is as described in Table 1. The hyperbolic model was selected for the first and fourth soil layers. As shown in Table 1, the strength parameters for the hyperbolic model were obtained directly from conventional triaxial tests. Except for parameter K, the other model parameters were determined using methods suggested by Duncan et al. (1980) and Wong and Broms (1989). Parameter K can be obtained better from back analysis based on field measurements rather than from laboratory tests, since it is bound to be strongly affected by sample disturbance. In this study, the stiffness modulus K was estimated based on the Young's modulus under small strain conditions according to the following equation:

$$[12] \quad K = \frac{2\beta}{P_a}\left(\frac{P_a}{\bar{p}}\right)^n \rho V_s^2 (1+\nu)$$

where ρ is density of the soil; V_s is shear-wave velocity; P_a is atmospheric pressure; $\bar{p}$ is the mean effective stress, and β is a reduction factor, which accounts for the difference between small deformation from seismic surveys and large deformation. For most excavation problems, β can be set equal to 0.5.

The shear-wave velocity can be estimated from seismic surveys or from correlations. According to Wu (1990), the shear-wave velocity for the Taipei silty sand can be found from the following correlation based on seismic survey:

$$[13] \quad V_s = 93.11(N+1)^{0.33}$$

where N, which is different from N in [1], is standard penetration resistance.

The second and third soil layers, which are virtually normally consolidated clayey soils, were simulated with the Modified Cam-clay model. The slope M of the critical state line was determined from the conventional triaxial test, λ and κ were determined from the one-dimensional consolidation test, and e_{cs} was estimated from the void ratio of the

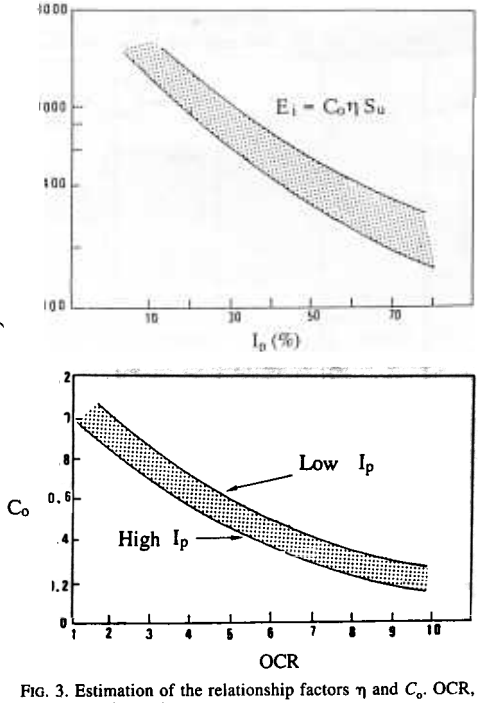

FIG. 3. Estimation of the relationship factors η and C_o. OCR, overconsolidation ratio.

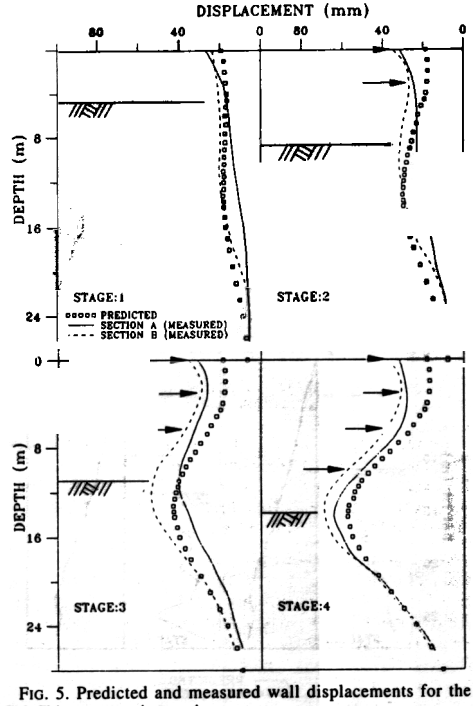

FIG. 5. Predicted and measured wall displacements for the Chi-Ching excavation project.

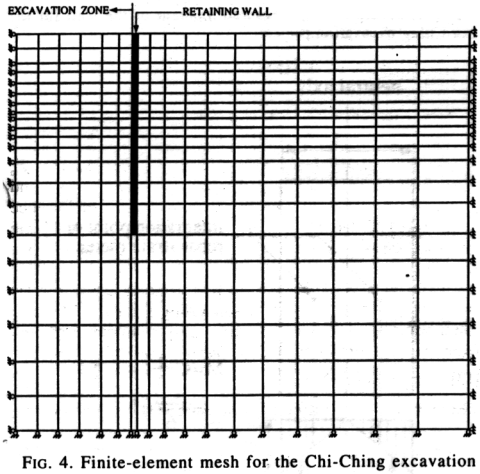

FIG. 4. Finite-element mesh for the Chi-Ching excavation project.

soil according to the following equation based on the Modified Cam-clay theory:

$$[14] \quad e_{cs} = e + \kappa \ln \bar{p} + (\lambda - \kappa) \ln \frac{\bar{p}_c}{2}$$

where p_c is preconsolidated pressure.

The elastic shear modulus G can be obtained through either special laboratory tests or field tests, or estimated using the following equation:

$$[15] \quad \frac{G}{S_u} = \frac{C_o \eta}{2(1+\nu)}$$

where C_o and η are relationship factors in the formula $E_i = C_o \eta S_u$, where E_i is initial Young's modulus; and S_u is undrained shear strength. Chang and Mohd (1980) suggested that η and C_o be estimated based on the plasticity index I_p and overconsolidation ratio, respectively, as shown in Fig. 3, which was drawn based on the results from Chang and Mohd (1980). If the analysis is performed using half the value obtained from [15], reasonable results are obtained. Although the proposed determination procedure was based on empirical correlations, it yielded consistent and reasonable results. Otherwise, a special laboratory testing technique, which is still in the research stage, would be required to determine G.

The values of plasticity index for the second and third soil layers at the site are 17.0 and 12.0, respectively, from which the value of G/S_u was obtained. All of the input values for the Modified Cam-clay model are listed in Table 1.

The analysis was carried out following the actual exca-

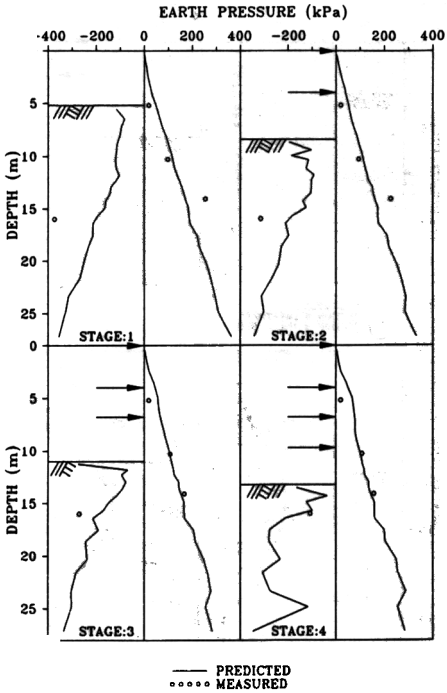

FIG. 6. Predicted and measured lateral earth pressure on the wall for the Chi-Ching excavation project.

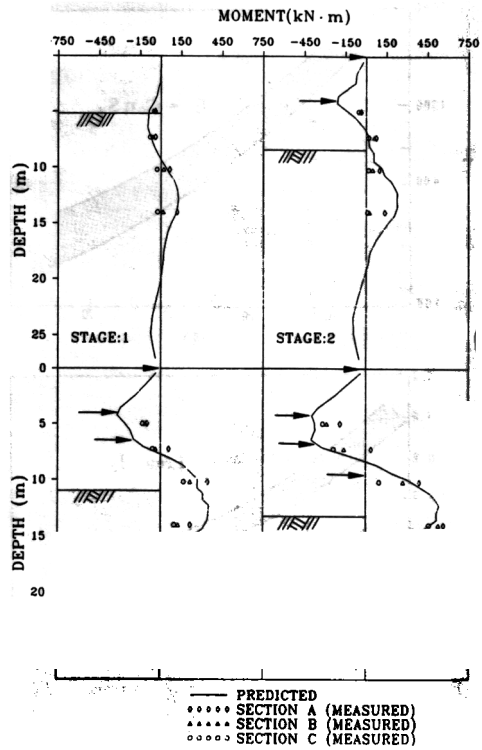

FIG. 7. Predicted and measured moment of the wall for the Chi-Ching excavation project.

vation sequence. Since trench excavation usually causes a rugged boundary surface between a trench and soil, the diaphragm wall surface would be expected to be very rough. Therefore, it is assumed that there is no relative displacement between the soil and concrete wall during analysis. Figure 4 shows the finite-element mesh used for analysis. Comparison of the calculated and observed wall displacements at two sections of the opposite sides is shown in Fig. 5. Comparison of the calculated and observed lateral earth pressures at one section of the side is shown in Fig. 6. Comparison of the calculated and observed wall bending moments at three sections of the opposite sides is shown in Fig. 7. It should be noted that the results obtained both from finite-element analysis and the rebar strain meter represent the stress of a point in concrete. The wall bending moment was calculated based on the assumption that the variation of stress over a cross section of the wall is linear. The calculation procedure either from analysis or from the rebar strain meter is shown in Fig. 8. It can be seen from the figures that the results of the analyses are close to the field observations.

The Chi-Chyang building

The Chi-Chyang building in Taipei has a maximum excavation depth of 13.6 m. The thickness and penetration depth of the diaphragm wall are 70 cm and 14.4 m, respectively. The excavation was completed using the top-down method in four excavation stages. The first three excavation stages

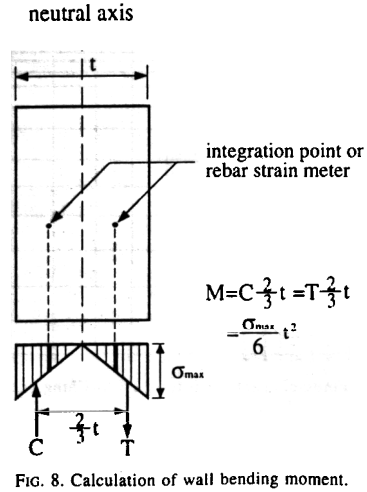

FIG. 8. Calculation of wall bending moment.

TABLE 2. Model parameters for the Taipei World Trade Center office building site

Soil parameter	Clayey silt, backfill (0–2.9 m)	Silty clay (2.9–14 m)	Silty clay (14–23 m)	Silty clay (23–28.5 m)	Silty clay (28.5–44 m)
M	—	1.20	1.03	1.20	1.20
λ	—	0.174	0.188	0.148	0.174
κ	—	0.035	0.037	0.030	0.035
e_{cs}	—	1.38	1.44	1.38	1.44
G/S_u		110	130	380	330
$\bar{\nu}$	—	0.3	0.3	0.3	0.3
ν	—	0.49	0.49	0.49	0.49
$\bar{c}$ (kPa)	9.81	—	—	—	—
$\bar{\phi}$ (°)	30.0	—	—	—	
R_f	0.9	—		—	—
ν_i	0.4	—	—	—	—
ν_f	0.49	—	—	—	—
K	125	—	—	—	—
n	1.0	—	—	—	—
K_{ur}	125	—	—	—	—

NOTE: ν_f is Poisson's ratio at or near failure.

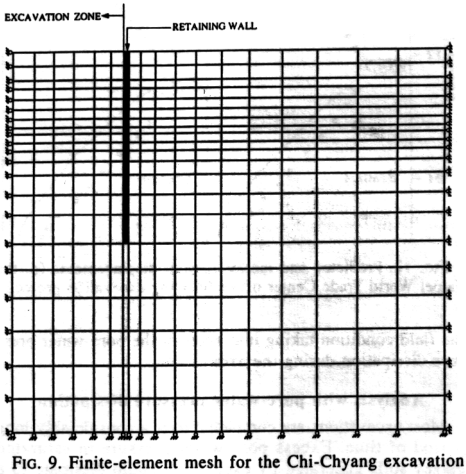

FIG. 9. Finite-element mesh for the Chi-Chyang excavation project.

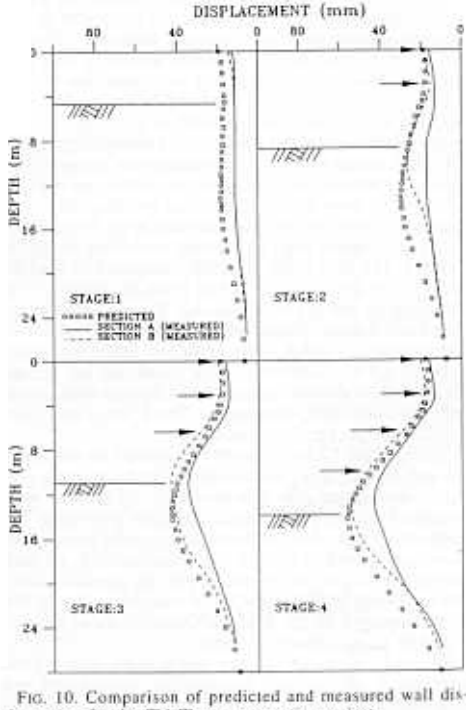

FIG. 10. Comparison of predicted and measured wall displacements for the Chi-Chyang excavation project.

were supported by the concrete floor slab, and the final stage was supported using temporary steel struts. The groundwater level was originally 3 m below ground surface; it was lowered to 8.6 m depth at the excavation side before the excavation was started and then lowered further to a depth of 12.0 m at the third excavation stage. The building site is also rectangular, but only a 34.0 m width of a section was used in this study. Wall deformation was measured down to 26 m below the ground surface using an inclinometer at both sides.

The geological conditions at the site are similar to those at the Chi-Ching building site. Therefore the parameters listed in Table 1 were also used for the case of the Chi-Chyang building, as were the material properties for the diaphragm wall. The axial stiffnesses of the concrete slab and the temporary steel strut based on actual material properties were 98 100 and 19 620 kN/m, respectively. Figure 9 shows the finite-element mesh used for the analysis. Q8 element was selected for the soil and diaphragm wall in the analysis. No relative displacement between the wall and soil was assumed. Comparison of the calculated and the observed wall displacements at two sections on opposite sides of the excavation is shown in Fig. 10. It can be seen from the figure that the calculated values are close to the observed values.

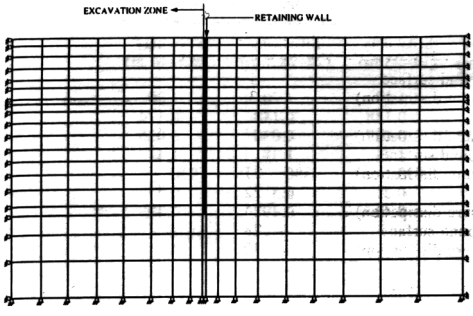

FIG. 11. Finite-element mesh for the Taipei World Trade Center office building excavation project.

The Taipei World Trade Center office building

The Taipei World Trade Center office building has a final excavation depth of 14.1 m, which was completed in five excavation stages using the bottom-up method of construction. A diaphragm wall 70 cm thick and 30 m long supported by four levels of temporary steel struts was used as the earth retaining structure. The building site is nearly rectangular. In this case, a 64.8 m width of a section was used in the analysis. Wall deformation was measured over the full depth of the wall using an inclinometer at one of the sides. The material properties for the diaphragm wall are the same as those for the Chi-Ching building. The axial stiffness for each level of strut was taken to be 14720 kN/m.

The parameters used in the soil model are shown in Table 2. The first layer, which is composed of backfill and soft silt deposits with low to medium plasticity, was simulated by the hyperbolic model. The strength parameters $\bar{c}$ and $\bar{\phi}$ were obtained from conventional triaxial tests. The parameters n and R_f in the hyperbolic model were taken to be 1.0 and 0.9, respectively. These values take into account the normalized material properties and flexible stress–strain behavior of the soil, respectively. The K value was taken as 125 based on previous studies.

The Modified Cam-clay model was selected for the rest of the soil layers, which are considered to be near the normally consolidated state. The parameters M, λ, and κ were obtained from laboratory tests as described previously. The value of e_{cs} was obtained based on the void ratio of the in situ soil according to [14]. The parameter G/S_u for each cohesive soil layer was estimated from the plasticity index and considering an OCR value of 1.0 according to Fig. 3. The input parameters for the Modified Cam-clay model for each soil layer are also shown in Table 2.

Figure 11 shows the finite element mesh used for the analysis. A Q8 element was selected for the soil and diaphragm wall. No relative displacement between the wall and soil was assumed. Comparison of the calculated and observed wall displacements for each excavation stage is shown in Fig. 12. It can be seen that for each stage of excavation, the calculated displacements of the retaining wall deviate slightly from the observed values. The reason may be that the soil, which has a very high silt content and had been exposed for about 2 months of the excavation period, did not actually behave as totally undrained, as assumed in the analysis. The following section describes a simulation of the field condition taking into account the pore-water pressure dissipation during the excavation.

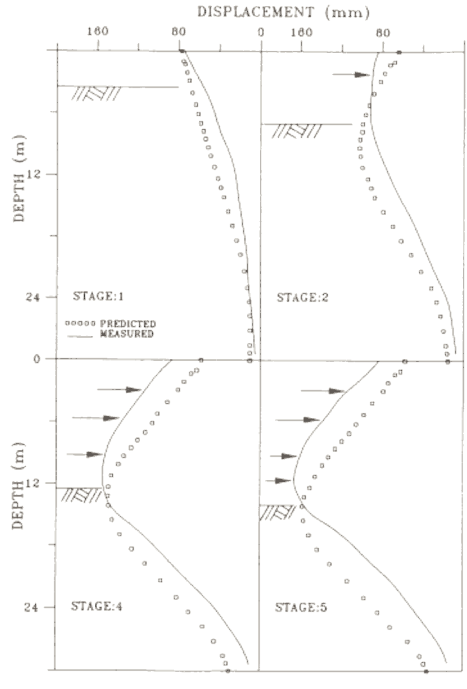

FIG. 12. Predicted and measured wall displacements for the Taipei World Trade Center office building excavation project.

Analysis with pore-water pressure dissipation

Most excavations are completed over a considerably long period of time. Excess pore-water pressure in saturated clayey soils generated by excavation could dissipate to a certain degree within such a period. Hence, wall displacement and ground-surface settlement obtained from undrained analysis could differ from actual field results. For this reason, the Taipei World Trade Center office building excavation project was reanalyzed to study the effect of pore-water pressure dissipation on excavation behavior.

The finite-element mesh for this study is the same as that shown in Fig. 11. The eight-node quadrilateral element with a pore-water pressure degree of freedom at each corner (Q8P4 element) was selected for clay soils, and a Q8 element was selected for the backfill material (silt) and diaphragm wall. It is noted that the vertical hydraulic boundaries outside the excavation zone were assumed to be fixed (i.e., constant) in the analysis. The vertical hydraulic boundaries inside the excavation zone and a base were assumed to be free (i.e., variable). Each stage in the finite-element simulation and related construction phases of the excavation project are listed in Table 3. The coefficient of horizontal permeability K_h was set equal to 50 times the coefficient of vertical permeability K_v to account for the presence of some sand

TABLE 3. Finite-element simulation of excavation stage

Stage	Description	Construction days
.	Excavated to 2.95 m below ground surface	.
2	Elapsed time (pore-water pressure dissipation)	3
3	First level of strut installed	4
4	Elapsed time (pore-water pressure dissipation)	16
5	Excavated to 7.00 m below ground surface	19
6	Elapsed time (pore-water pressure dissipation)	21
7	Second level of strut installed	22
8	Elapsed time (pore-water pressure dissipation)	24
9	Excavated to 10.1 m below ground surface	28
10	Elapsed time (pore-water pressure dissipation)	30
11	Third level of strut installed	31
12	Elapsed time (pore-water pressure dissipation)	36
13	Excavated to 12.3 m below ground surface	40
14	Elapsed time (pore-water pressure dissipation)	42
15	Fourth level of strut installed	43
16	Elapsed time (pore-water pressure dissipation)	44
17	Excavated to 14.1 m below ground surface	47

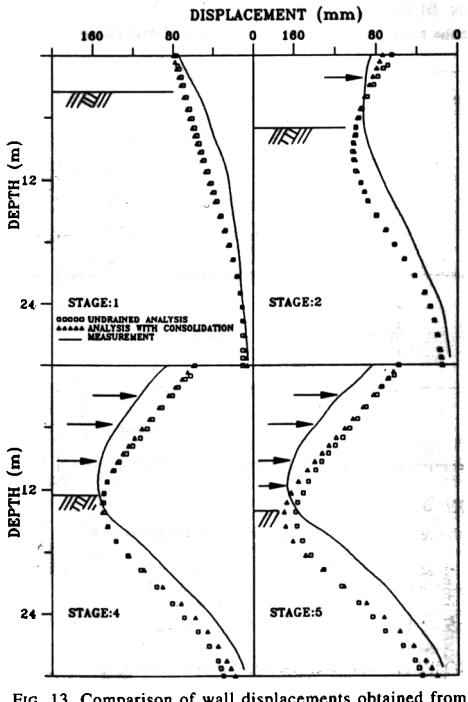

FIG. 13. Comparison of wall displacements obtained from undrained analysis, field measurement, and analysis considering the effect of consolidation.

seams, which may exist in the site and accelerate dissipation of excess pore-water pressure. Figure 13 shows the comparison of wall displacements obtained from undrained analysis, field observation, and analysis considering pore-water pressure dissipation. As seen from the figure, the displacement of the wall during intermediate excavation stages for both the undrained analysis and the analysis considering consolidation effects are similar. However, at the final excavation stage when the effect of consolidation is more obvious, the displacement of the wall from the undrained analysis approximates the field measurement to a lesser degree. Thus, the analysis considering pore-water pressure dissipation yields better results.

Figures 14 and 15 show the variation of pore-water pressure obtained from the analysis at three different depths on the passive and active sides of the wall, respectively, based on actual construction duration. It can be seen that the unloading pressure generated by excavation has caused the decrease of pore-water pressure at each side of the retaining wall. The change of pore-water pressure at a certain point in the soil is related to the distance of the point from the excavation boundary. The shorter the distance from the excavation boundary, the more intense is the change in pore-water pressure. It can also be seen from the figure that pore-water pressure increases gradually with elapsed time. This may be due to the dissipation of excess pore-water pressure before commencement of the next stages of excavation. However, in this case pore-water pressure only increases slightly during the elapsed time for each construction phase because of the short duration of each phase and the absence of drained material in the clayey soil. Thus the analysis is not much different from that of the totally undrained case, although the in situ clayey soil has a high silt content (I_p ranges from 20 to 25).

To understand the deformation trends of the retaining wall and soil after the completion of excavation, analysis with the consideration of pore-water pressure dissipation was carried out, as shown in Figs. 16 and 17. It shows that the maximum displacement of the retaining wall can decrease by a small amount with elapsed time after the completion of excavation. Likewise, the ground-surface settlement decreases with elapsed time after completion of excavation, as illustrated in Fig. 17. This may be because the excavation generates larger negative excess pore-water pressure in the soil on the passive side of the retaining wall (Fig. 14) and less negative excess pore-water pressure on the active side (Fig. 15). The dissipation of negative excess pore-water

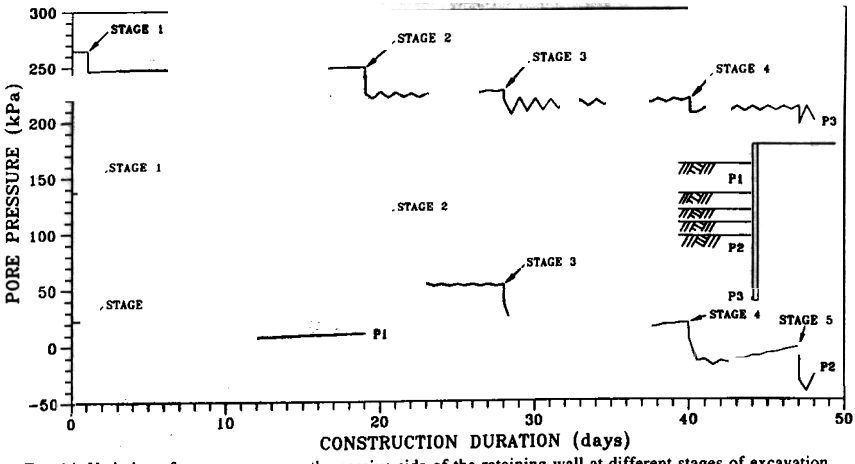

FIG. 14. Variation of pore pressure on the passive side of the retaining wall at different stages of excavation.

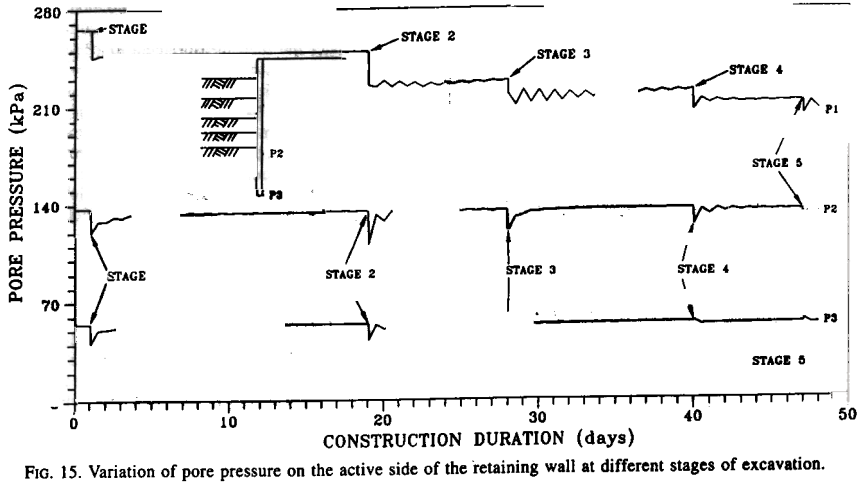

FIG. 15. Variation of pore pressure on the active side of the retaining wall at different stages of excavation.

pressure on the passive side of the retaining wall causes the soil to swell. This results in the decrease of the wall displacement, which in turn causes the ground surface to rebound a little.

Since there are no case histories available, the results from the analyses cannot be compared with field observations. However, the phenomenon obtained from the analysis is similar to Padfield and Mair's (1984) observation. The analysis has a significant meaning in engineering practice, especially for excavation in urban areas where the safety of adjacent buildings is a major concern. Based on the results from the analysis, additional ground settlement after the completion of excavation may not occur causing further building damage as long as the creep effect in the clayey soil is not obvious.

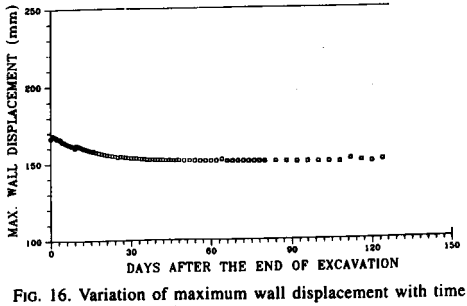

FIG. 16. Variation of maximum wall displacement with time after the end of excavation.

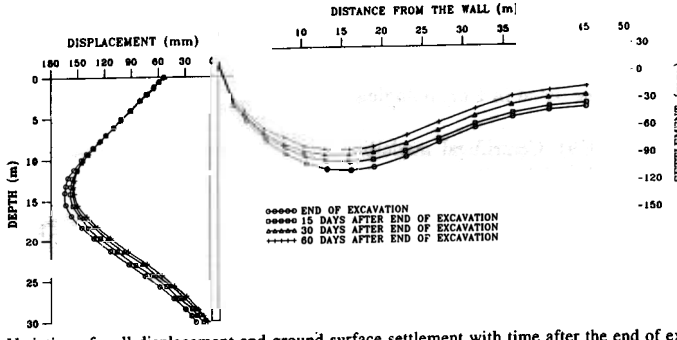

FIG. 17. Variation of wall displacement and ground-surface settlement with time after the end of excavation.

Conclusions

Because of the effects of sample disturbance, some of the soil parameters obtained from the laboratory test usually would not give reliable predictions in finite-element analysis. For this reason, field measurements are normally used to calibrate the results of finite-element analyses to obtain more representative parameters of the in situ soil. This process depends heavily on professional experience and subjective judgement. In this study, an application of the finite-element analysis to deep excavation in layered sandy and clayey soil deposits using the combination of the hyperbolic and the Modified Cam-clay models was proposed. In the analysis, the drained behavior of cohesionless soil was simulated using the hyperbolic model, and the undrained behavior of cohesive soil was simulated using the Modified Cam-clay model. A rational procedure for determining soil parameters for both models was proposed. Based on the case studies, it can be seen that the results from finite-element analyses are fairly close to those from field observations. All of the analyses were strictly based on the parameter determination procedures established. In addition, the following conclusions can be made.

(1) For excavations with a long construction period, analysis considering pore-water pressure dissipation can give better predictions than using totally undrained analysis. However, for the case of a short period of construction and absence of drained material in the clayey layer, the excavation behavior is close to that of the totally undrained behavior.

(2) Based on parametric studies, the pore-water pressure on the passive side of the retaining wall experiences an abrupt decrease immediately after excavation and then gradually recovers with elapsed time. On the other hand, the pore-water pressure on the active side of the retaining wall does not experience significant change during excavation. Pore-water dissipation after the completion of excavation can cause a decrease in the final wall deformation and ground-surface settlement. It should be noted that the creep effect of clayey soil on excavation was not considered in the analysis.

Biot, M.A. 1941. General theory of three dimensional consolidation. Journal of Applied Physics, **12**: 155–169.

Britto, A.M., and Gunn, M.J. 1987. Critical state soil mechanics via finite elements. Ellis Horwood Limited, Chichester, U.K.

Brown, P.T., and Booker, J.R. 1985. Finite element analysis of excavation. Computers and Geotechnics, **1**: 207–220.

Chang, C.S., and Mohd, H.B.A. 1980. Deformation analysis for braced excavation in clay. *In* Proceedings of the Symposium on Limit Equilibrium, Plasticity and Generalized Stress Strain Applications in Geotechnical Engineering. *Edited by* Young and Selig. ASCE, Hollywood, Florida, pp. 205–225.

Clough, G.W., and Mana, A.I. 1976. Lessons learned in finite element analysis of temporary excavation in soft clay. *In* Numerical method in geomechanics. 3rd ed. *Edited by* Desia. Blacksburg Va., pp. 496–510.

Duncan, J.M., and Chang, C.Y. 1970. Nonlinear analysis of stress and strain in soils. ASCE Journal of the Soil Mechanics and Foundations Division, **94**(SM 5): 637–659.

Duncan, J.M., Byune, P., Wong, K.S., and Mabry, P. 1980. Strength, stress–strain and bulk modulus parameters for finite element analysis of stresses and movements in soil masses. University of California, Berkeley, Department of Civil Engineering, Report No. UCB/GT/80-01.

Finno, R.J. 1983. Response of cohesive soil to advanced shield tunneling. Ph.D. dissertation, Stanford University, Stanford, Calif.

Ghaboussi, J., and Pecknold, D.A. 1984. Finite element analysis of geometrically altered structures. International Journal for Numerical Methods in Engineeering, **20**: 2051–2064.

Ishihara, K. 1970. Relations between process of cutting and uniqueness of solutions. Soils and Foundations, **10**(3): 50–65.

Johnston, P.R. 1981. Finite element consolidation analysis of tunnel behavior in clay. Ph.D. dissertation, Stanford University, Stanford, Calif.

Moh and Associates. 1982. Report on instrumentation monitoring of five deep excavations in the Taipei City. Taipei Mass Rapid Transit Bureau, Taipei, Taiwan. Report No. 219-1. pp. 1–149.

Padfield, C.J., and Mair, R.J. 1984. Design of retaining walls embedded in stiff clay. Construction Industry Research and Information Association, London, U.K., Report No. 104, pp. 83–84.

Roscoe, K.H., and Burland, J.B. 1968. On the generalized stress strain behavior of "wet" clay. *In* Engineering plasticity. *Edited by* Heyman and Leckie. Cambridge, pp. 535–609.

Small, J.L., Booker, J.R., and Davis, E.H. 1976. Elasto-plastic consolidation of soil. International Journal of Solids and Structures, **12**: 431–448.

Wong, K.S., and Broms, B.B. 1989. Lateral deflection of braced excavation in clays. ASCE Journal of Geotechnical Engineering, **115**: 853–870.

Wu, C.M. 1990. Investigation of shear wave velocity in Taiwan area using down hole test. M.Eng. thesis, Department of Construction Engineering, National Taiwan Institute of Technology, Taipei, Taiwan, Republic of China.